Atmospheric neutrino flux above 1 GeV

Vivek Agrawal,[1] T.K. Gaisser,[1] Paolo Lipari,[2] and Todor Stanev[1]
[1]*Bartol Research Institute, University of Delaware, Newark, Delaware 19716*
[2]*Dipartimento di Fisica, Università di Roma, Piazzale Aldo Moro 2, Rome, Italy*
(Received 13 July 1995)

In this paper we extend an earlier calculation of the flux of atmospheric neutrinos to higher energy. The earlier calculation of the neutrino flux below 3 GeV has been used for calculation of the rate of contained neutrino interactions in deep underground detectors. The fluxes are needed up to neutrino energies of 10 TeV to calculate the expected rate of neutrino-induced muons passing into and through large, deep detectors. We compare our results with several other calculations, and we evaluate the uncertainty in the rate of neutrino-induced muons due to uncertainties in the neutrino flux.

PACS number(s): 96.40.Tv, 14.60.Pq, 95.85.Ry

I. INTRODUCTION

In the past few years several groups have reported new measurements of ν-induced muons passing through large, deep-underground detectors [1–6]. These measurements provide better statistics than the earlier pioneering measurements at KGF [7] and in South Africa [8], but the results and their interpretation remain ambiguous, in part because of the intrinsic difficulty of the measurement but in part because of differences in the calculations used to interpret the measurements. In particular, the relation of these measurements to the anomalous flavor ratio of contained interactions of atmospheric neutrinos [9, 10] is still controversial.

Interpretation of the flux of neutrino-induced muons depends on an absolute comparison between a measured rate and a calculated intensity. The calculation contains three essential ingredients: propagation of muons after they are produced in charged-current interactions of ν_μ and $\bar{\nu}_\mu$; the energy spectrum of muons produced in charged-current interactions of neutrinos as well as the magnitude of the cross section; and the flux of atmospheric neutrinos itself. The first factor in the calculation is well understood, and different calculations give similar results [11, 12]. The uncertainty in the cross section is discussed in recent papers [13–15]. In this paper we discuss the calculation of the neutrino flux in the energy range relevant for neutrino-induced muons; that is, from one GeV up to 10^4 GeV of neutrino energy. The calculated flux of neutrinos and muons given here is essentially an extension of the low energy calculation [16] that has been used extensively for evaluation of the rate of contained neutrino interactions. In this paper we also give a critical discussion of the sources of uncertainty in the calculation, as well as a comparison of these results to those of other calculations.

The neutrino flux depends on the primary cosmic-ray spectrum and on the production of pions and kaons by interactions of cosmic-ray hadrons in the atmosphere. Because of the close relationship between neutrino and muon fluxes, we tabulate both fluxes. We also discuss the extent to which measurements of the muon flux place constraints on the neutrino flux. We begin in Sec. II with a discussion of the primary spectrum and its uncertainties. Then in Sec. III we discuss the inclusive cross sections that determine the production of muons and neutrinos in the atmospheric cosmic-ray cascading. Section IV contains the neutrino and muon fluxes in tabular form. In the conclusion we compare this calculation with others and summarize our assessment of the uncertainty in the atmospheric neutrino flux.

II. PRIMARY SPECTRUM

The cosmic-ray spectrum incident on the atmosphere consists of protons and nuclei. To a first approximation the uncorrelated spectra of atmospheric secondaries, such as neutrinos and muons, depend only on the number of incident nucleons in the primary spectrum as a function of energy per nucleon [17]. We call this the all-nucleon spectrum. The range of neutrino energies important for ν-induced muons is $1 \leq E_\nu \leq 10^4$ GeV, as shown, for example in Fig. 2 of Ref. [13]. The corresponding range of primary energy per nucleon is about a factor of ten higher, as illustrated in Fig. 1. Approximately 85% of neutrino-induced muons come from primary nucleons with energies less than 10^4 GeV. (The exact fraction depends somewhat on the angle as shown in Fig. 1.)

In this energy range, the all-nucleon spectrum is dominated by hydrogen and helium, even in the case of extrapolations in which the spectrum in total energy per nucleus (the so-called "all-particle" spectrum) is dominated by heavy nuclei at higher energy. The relative contribution of different nuclei to the all-nucleon spectrum is discussed in Ref. [18], where it is shown, for example, that hydrogen contributes about 81 (68) % of the intensity at 10 (10^4) GeV and helium 72 (70) % of the remainder. Thus the overall uncertainty is dominated by the uncertainty in the measurements of the spectrum of hydrogen. The fraction of helium is crucial for determining the charge ratio of muons and the $\nu/\bar{\nu}$ ratios because this is the origin of most of the incident neutrons. Heavy nuclei may become more important around 10^5 GeV/nucleon, as noted below.

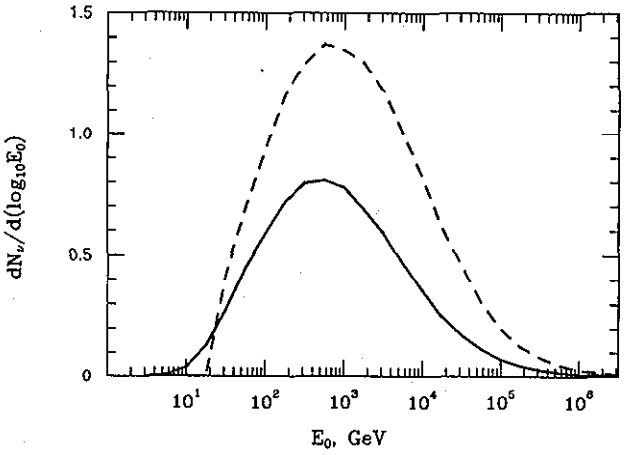

FIG. 1. Primary cosmic-ray nucleon energy contribution to the upward-going neutrino induced muon flux (E_μ >1 GeV). The solid line is for cos(θ)=–1 and the dashed is for cos(θ)=–0.15.

Figure 2 shows the data summary from Ref. [18] of the direct measurements of the primary protons, helium and heavier nuclei made with various balloon and satellite experiments. There are two measurements of the spectrum of hydrogen [19, 20] in the 10–100 GeV range that differ in normalization by about 30%, an amount which is larger than the statistical error of either experiment. Up to about 10^4 GeV, the envelope of the measurements also covers a range of about 30%. Thus we assign an uncertainty of ±15% to the all-nucleon spectrum in this entire energy range.

At higher energy the uncertainty of the cosmic-ray composition plays a bigger role. The data of JACEE [23, 24] (shown by the filled circles in Fig. 2) have two main features — a downward bend in the proton spectrum and an increase of the contribution of all-nuclei heavier than helium. These two effects tend to compensate each other and leave the slope of the all-nucleon spectrum unchanged up to 10^5 GeV. If, however, the bend of the proton spectrum is real but the flattening of the spectra of the heavy nuclei is not, there will be a corresponding steepening of the all-nucleon spectrum around 10^4 GeV. These two possibilities are indicated in Fig. 2. Since primaries with $E > 10^4$ GeV/nucleon contribute only about 15% of the flux of upward muons, however, uncertainties at the level of 20 – 30 % above this energy increase the uncertainty in the upward muon rate only by a few percent.

For the calculations in this paper we use the all-nucleon spectrum with the higher extrapolation, which corresponds to the dash-dotted curves in Fig. 2. This primary spectrum was based originally on an analysis of the data summary of Garcia-Munoz and Simpson [33] done for the calculation of Ref. [16]. It is extended to higher energy [18] by including data from the summary of Swordy [34] and other more recent data. At energies above 10^4 GeV/nucleon we use only the measurements of JACEE [23,24], shown with filled circles in Fig. 2. In Fig. 3 we compare the nucleon spectrum used for this calculation with the other fit to the data of Fig. 2 and with the spectra used in other calculations of the neutrino flux at high energy.

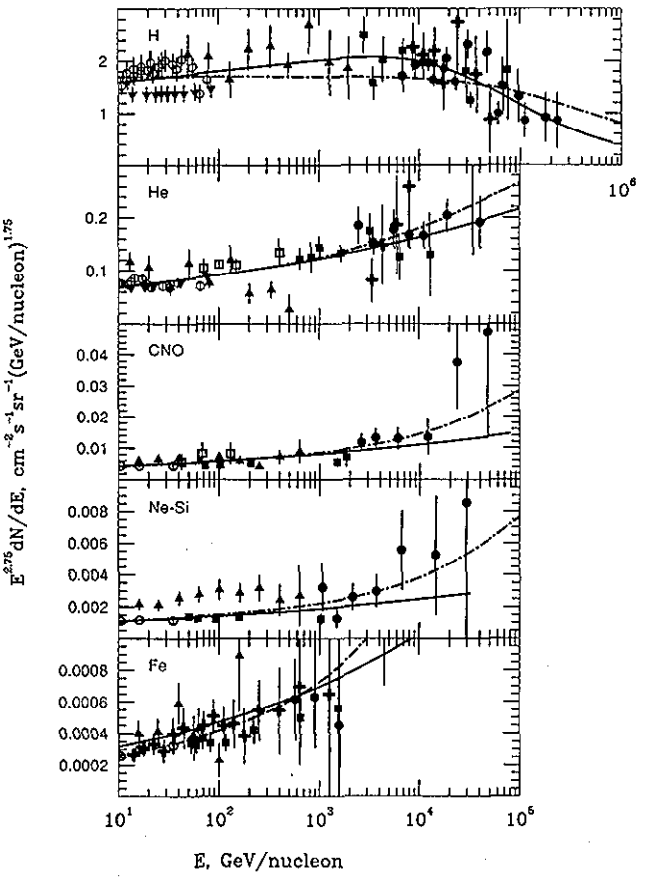

FIG. 2. Direct data on the spectra of different cosmic-ray nuclei. The data for H and He are from: open circles, Ref. [19]; inverted triangles, Ref. [20]; triangles, Ref. [21]; filled squares, Ref. [22]; filled circles, Refs. [23, 24]; crosses, Ref. [25]; hexagons, Ref. [26]; and open squares, Ref. [27]. The data for heavier nuclei are from: open circles, Ref. [28]; triangles, Ref. [29]; open squares, Ref. [30]; filled squares, Ref. [31]; crosses, Ref. [32]; and filled circles, Ref. [24]. The lines represent the two fits discussed in the text: (1) (solid line) steepening H and all nucleon spectrum; (2) (dash-dotted) a gradual bending of the H spectrum which is compensated by flattening of the spectra of all heavier nuclei.

The low energy part of the spectrum (< 20 GeV) is affected by the geomagnetic field and by modulation by the solar wind, both of which prevent some fraction of the low energy galactic cosmic rays from reaching the atmosphere to produce secondaries. These effects are of greatest importance for the ~ GeV neutrino flux that is responsible for contained neutrino interactions, but they also have some importance for neutrino-induced muons, especially for muons that enter and stop in the detector. A new evaluation of the geomagnetic cutoffs is the subject of Ref. [39]. We tabulate below the reduction in neutrino flux due to the geomagnetic cutoffs at several detector locations.

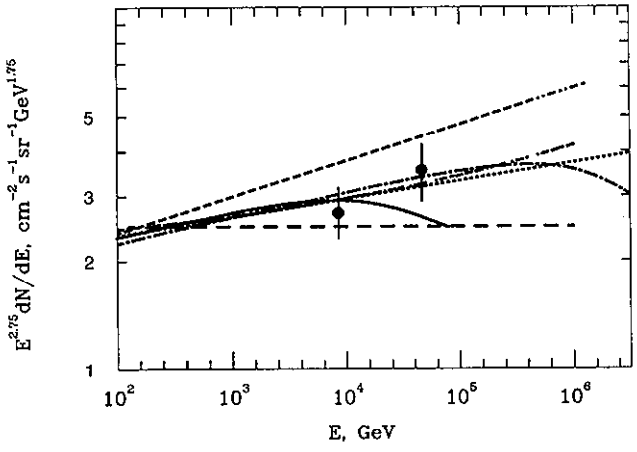

FIG. 3. The all-nucleon spectra derived from the fits from Fig. 2 (same line coding) compared with spectra used in other neutrino flux calculations: short dashed, Ref. [35]; long dashed, Ref. [36]; dotted, Ref. [37]; and short-long dashed, Ref. [38]. The two data points are from the JACEE data set [23, 24].

III. HADRON PRODUCTION

To calculate the atmospheric cascade we use a model of hadronic interactions called TARGET that is essentially the same as originally used in Ref. [16] for calculation of the neutrino flux below 3 GeV. It is based on a parametrization of particle interactions on targets of different mass [40]. It is tuned to describe correctly different sets of experimental data in the tens [41–43] to hundreds of GeV [44] range of lab energy. The original version of this model is described in Ref. [45]. The only significant change since the calculation [16] concerns the description of the production of strange hadrons at high energy. The description of the production and decay of resonances in the GeV region was also improved. The neutrino fluxes below 3 GeV are indistinguishable from those of Ref. [16] in the absence of geomagnetic cutoffs. A change in the production of kaons in interactions with energy above 1000 GeV leads to an increase of the neutrino flux in the TeV region relative to a preliminary version of this calculation used in Ref. [13]. On the other hand, the assumptions of this model about kaon production on nuclear targets at high energy are at the higher end of the experimental range and may overestimate kaon production around 1 TeV and above. The uncertainty about production of kaons at high energy is a principal source of uncertainty in the model which we discuss later.

To get an idea of the uncertainties in the neutrino fluxes that arise from uncertainties in the description of hadronic interactions it is useful to characterize the inclusive cross sections by their moments, weighted by the shape of the primary spectrum. For example, the contribution of pions is approximately proportional to

$$Z_{p\pi^{\pm}} = \int_0^1 x^{\gamma} \frac{dN_{p\pi}}{dx}\, dx, \qquad (1)$$

where dN/dx is the distribution of charged pions produced in collisions of protons with nuclei in the atmosphere, $x = E_\pi/E_p$ and γ is the integral spectral index of the primary cosmic-ray spectrum. The corresponding factors $Z_{pK^{\pm}}$ (for production of charged kaons), Z_{pK^0}, $Z_{p\pi^0}$, Z_{pp}, etc., are defined analogously.

These spectrum weighted moments appear explicitly in analytic approximations to the uncorrelated particle fluxes in the atmosphere [46, 47]. Inspection of the analytic approximations for neutrino and muon fluxes from power-law primary spectra is sufficient to determine which are the most important sources of uncertainty in different ranges of primary energy [48]. For vertically incident leptons with energy below 100 GeV, approximately 95% of muons and 65% of ν_μ come from pions, whereas above 1000 GeV about 50% of muons but less than $\sim$ 10% of ν_μ come from decay of pions. Most of the remainder come from decay of charged kaons. (For horizontal leptons this transition region is shifted to higher energy [47], so that kaons are less important for production of horizontal ν_μ-induced muons.)

The relative importance of kaons for production of neutrinos at high energy is a consequence of the kinematics of meson decay coupled with the steep primary spectrum, as explained in Ref. [48]. In the low energy region, the uncertainties in both the muon and the neutrino fluxes are dominated by the uncertainty in pion production, as represented by $Z_{p\pi}$. At high energy the dominant source of uncertainty in the neutrino flux is kaon production, but this is not the case for muons. As a consequence, the extent to which measurement of the atmospheric muon spectrum can be used to normalize the neutrino spectrum is limited.

With this background, we now compare the Z factors as estimated from various sets of data and as represented in the TARGET model. We also quote the Z factors used for some other calculations [52, 53] of the fluxes of high energy neutrinos, where available. The first six lines of Table I [54] show estimates of the Z factors and related parameters based on three data sets for proton-proton collisions at energies from 175 GeV [49] to 400 GeV [50] on fixed targets and from the CERN Intersecting Storage Rings (ISR) [51] equivalent to lab energy of $\sim$ 1500 GeV. The second and third columns are estimates of the spectrum-weighted moments. Column 4 is a tabulation of $R_{K/\pi} = Z_{pK^{\pm}}/Z_{p\pi^{\pm}}$. The factors $\mathcal{E}(i)$ will be discussed below.

Two estimates of the parameters are given for each of the three data sets in Table I. For the data of Ref. [49] the first line comes from the parametrization given in that reference, and the second line from the fit that we performed to the data points. For Ref. [50] the first line is from direct integration of all data points, and the second excludes the contribution from $x > 0.6$, where the measurements show a strange feature (possibly due to a contamination of protons in the samples of positive mesons). For Ref. [51] the first line is from the analysis of Perkins [55] and the second from Ref. [56].

In addition to differences among the moments obtained from data on hydrogen targets, there is also the uncertainty associated with the relation between inclusive

TABLE I. Comparison of Z factors.

Reference	$Z_{p\pi^\pm}$	$Z_{pK^\pm}$	$R_{K/\pi}$	$\mathcal{E}(\mu)$	$\mathcal{E}(\nu_\mu)$	$\mathcal{E}(\nu_e)$
[49] (175 GeV)	0.074	0.0086	0.12	10.03	2.47	0.078
	0.076	0.0097	0.13	10.54	2.73	0.087
[50] (400 GeV)	0.079	0.0074	0.09	10.22	2.23	0.068
	0.074	0.0074	0.10	9.70	2.20	0.068
[51] (1500 GeV)	0.083	0.0086	0.10	10.96	2.53	0.079
	0.083	0.0100	0.12	11.34	2.85	0.090
[52] (p-p)	0.072	0.0094	0.13	10.04	2.64	0.085
[52] (p-air)	0.069	0.0087	0.13	9.54	2.46	0.078
[53] (p-air)	0.065	0.010	0.15	9.47	2.72	0.089
TARGET (1000 GeV)	0.072	0.0105	0.15	10.34	2.89	0.094

cross sections on proton targets and cross sections on light nuclei. In one case where the same group took data on both hydrogen and nuclear targets, the inclusive cross sections at $p_T = 0.3$ GeV/c and $x = 0.3$ (as near to the peak of the integrand of Eq. (1) as possible with the nuclear target data [44]) are similar for the two types of targets. Comparison of Z factors calculated in an event generator which treats both pp and p-nucleus collisions (SIBYLL)[57] also shows negligible differences between the two.

On the other hand, studies of the A dependence of inclusive cross sections on a variety of nuclear targets (excluding hydrogen) do show significant variation in the fragmentation region, with a tendency for the K/π ratio to increase with target mass [41, 58, 59]. Production of both pions and kaons is enhanced in collisions on nuclear targets, but kaons may be more enhanced than pions.

Associated production of kaons through $p \to \Lambda K^+$ in the fragmentation region accounts for the large ratio of Z_{pK^+}/Z_{pK^-} since K^- are produced essentially only through K^+/K^- pair production in the central region. The analogous process for an incident neutron is $n \to \Lambda K^0$. In TARGET the incident nucleon has an energy-dependent probability to dissociate into a ΛK^+ pair, which is assumed to increase from threshold to 4.2% at 30 GeV/c, 6.5% at 300 GeV/c and asymptotically to 6.8%. By comparison, the integrated cross section in the forward fragmentation region for $p + \mathrm{Be} \to \Lambda + X$ at 300 GeV/c [60] is ~ 15 mb, which corresponds to a probability of 7.3% for $\sigma_{p\,\mathrm{Be}} = 206$ mb. The probability for Λ production in pp collisions is approximately 5 – 6 % in each hemisphere [61]. As a consequence of the extra channel available for production of positive kaons by protons, the inclusive cross section is significantly harder for K^+ than for K^- [62].

Production of K^+/K^- pairs is determined in TARGET by the energy-dependent multiplicity of K^- [63] with an assumed enhancement of 1.45 for target "air" nuclei ($A = 14.5$) [58]. The resulting distributions of produced $\pi^\pm$ and $K^\pm$ agree fairly well with the 19–24 GeV/c data [41,42]. In Fig. 4 we compare the distributions from TARGET for p-air interactions at 400 GeV/c with three sets of pp data (175, 400, and 1500 GeV/c). As described above, both pion and kaon production are enhanced at low x in TARGET, but kaons more so than pions. For $x > 0.2$ π^+ distributions from TARGET (for p-air collisions) are somewhat below the pp data and K^+ somewhat above.

The Z factors corresponding to TARGET are listed in Table I, along with the values from Refs. [52, 37] in which the scheme of Ref. [64] was used to relate pp to p air. The values used by Volkova [35] to calculate the

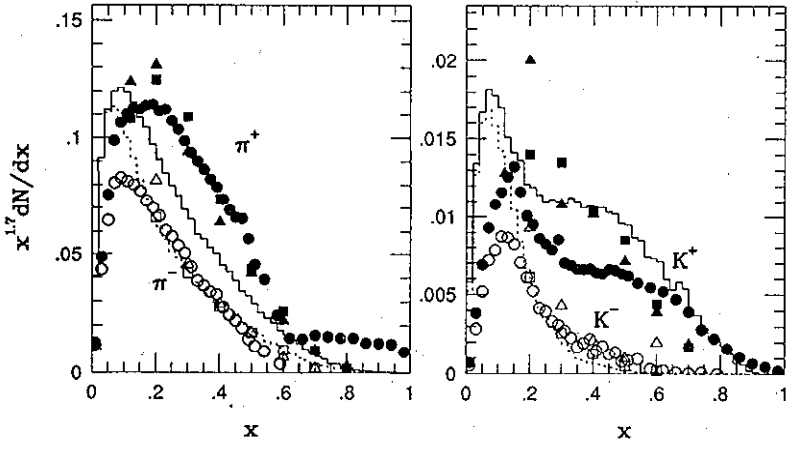

FIG. 4. Spectrum-weighted inclusive distributions for charged secondaries integrated over transverse momentum as derived from experimental data on pp ($\bar{p}p$) interactions at incident energy of 175 GeV (triangles) [49], 400 GeV (circles) [50], and an equivalent lab energy of 1500 GeV (ISR, squares) [51]. Distributions from the event generator TARGET for p-air collisions at 400 GeV are shown for comparison.

TABLE II. Z factors from the TARGET event generator for proton interactions on air nuclei for $\gamma = 1.7$.

E_p	Secondary particles							
(GeV)	p	π^+	π^-	K^+	K^-	π^0	K^0	n
3	0.4000	0.0239	0.0154	0.0001	0.0000	0.0200	0.0001	0.1013
10	0.2742	0.0529	0.0365	0.0014	0.0000	0.0447	0.0008	0.0352
10^2	0.2681	0.0456	0.0329	0.0072	0.0029	0.0390	0.0082	0.0335
10^3	0.2732	0.0414	0.0302	0.0079	0.0027	0.0356	0.0071	0.0372
10^4	0.2710	0.0405	0.0301	0.0076	0.0026	0.0346	0.0070	0.0369
10^5	0.2696	0.0409	0.0292	0.0076	0.0025	0.0346	0.0068	0.0372

flux of high energy atmospheric neutrinos are listed here from Ref. [53]. Considering all the estimates listed in Table I (for both pp and p air), the $Z_{p\pi^\pm}$ cover a range of approximately $\pm 12\%$. The corresponding range for $Z_{pK^\pm}$ is $\pm 17\%$. In the Conclusion we use these numbers to estimate the contribution of the uncertainties in the input to the neutrino flux calculations to the uncertainty in the expected flux of neutrino-induced muons.

The last three columns of Table I show the influence of these Z-factor sets on the estimates of the uncorrelated fluxes of muons and neutrinos. $\mathcal{E}(\mu)$, $\mathcal{E}(\nu_\mu)$, and $\mathcal{E}(\nu_e)$ are the coefficients for the asymptotic ratio of the vertical lepton flux to the primary cosmic flux in the relation $\Phi_l = \mathcal{E}_l \times \Phi_{\rm CR}/E_l$ [47]. At asymptotically high energy this form gives a good estimate of the actual muon and neutrino fluxes. The range of values is $\pm 8\%$ for muons and $\pm 14\%$ for neutrinos.

Finally, there is the question of the energy dependence of the Z factors, as shown in Table II for TARGET. For $E < 100$ GeV there is energy dependence (especially for production of strange particles) as the high energy, quasiscaling region is approached. The gross energy dependence of TARGET above 1000 GeV is determined by adjusting the model of Ref. [40] so that it also fits measurements of charged particles produced in interactions of 20 TeV protons in lucite [65] as described in Ref. [45]. The extrapolation reproduces the rise of the central rapidity plateau that continues to the energy range of $\bar{p}p$ colliders. Since there is no information on particle production in the fragmentation region above 1000 GeV, we make the assumption that the Z factors remain constant above this energy. This is the difference mentioned at the beginning of this section that leads to an increase in kaon production compared to the original version of TARGET.

To estimate the contribution of each Z factor to the overall uncertainty in the flux of $\nu_\mu + \bar{\nu}_\mu$ we used the analytic approximations for the neutrino fluxes from a power-law primary spectrum [46,47]. The result is shown as a function of energy in Fig. 5 for estimated maximum uncertainty in each of the various Z factors as tabulated in the last column of Table III. The other entries in Table III show the relative changes in the flux of $\nu_\mu + \bar{\nu}_\mu$ due to a fractional change in the corresponding Z factor. Most neutrino-induced upward muons are produced by neutrinos with $10 \leq E_{\nu_\mu} \leq 1000$ GeV. For this reason, the single most important factor is the uncertainty in $Z_{p\to K^+}$.

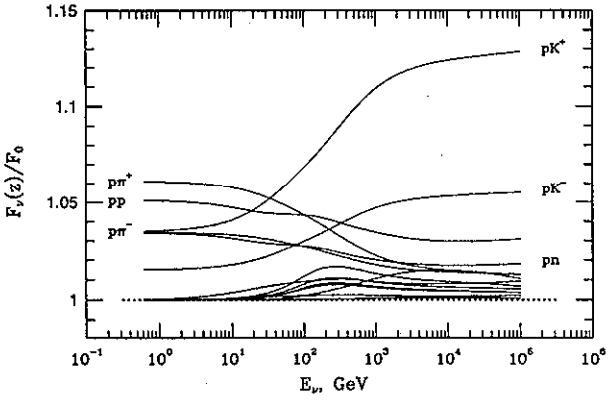

FIG. 5. Ratios of the $\nu_\mu + \bar{\nu}_\mu$ flux calculated with different Z factors increased by their maximum experimental uncertainty to the flux calculated with the central Z-factor values. The ratios are symmetric, i.e., inverted when the calculation is done with the lowest allowed Z-factor values.

TABLE III. Effect of different Z factors on the flux of muon neutrinos and antineutrinos. Only Z factors affecting the flux by more than 2% are included. The last column gives the maximum relative uncertainty deduced from experimental data and used for the estimate shown in Fig. 5.

Z	$\partial F(\nu_\mu + \bar{\nu}_\mu)/\partial \ln Z$			$\Delta Z/Z$
E_ν (GeV)	10	100	1000	
pp	0.338	0.307	0.310	0.14
pn	0.046	0.040	0.030	0.68
$p\pi^+$	0.482	0.359	0.186	0.12
$p\pi^-$	0.276	0.222	0.146	0.12
pK^+	0.163	0.273	0.436	0.25
pK^-	0.071	0.118	0.188	0.25
$\pi^+\pi^+$	0.019	0.047	0.048	0.19
π^+K^+	0.003	0.037	0.045	0.29
π^+K^-	0.002	0.020	0.024	0.25

IV. RESULTS OF THIS CALCULATION

The results of our calculation are presented in Tables IV–VI, for muons, ν_μ and ν_e, respectively. These fluxes correspond to the cosmic-ray spectrum at solar minimum and take no account of geomagnetic effects. The fluxes are tabulated at energies, for which other calculations [35, 37, 36, 38] have published their results. More detailed tables are available on request, which give the fluxes at intervals of 1/10 decade of energy. The fluxes for $E_{\rm lepton} < 1000$ GeV are obtained from a straightforward Monte Carlo calculation, selecting primary neutrons and protons from the spectrum. This has the consequence that statistical fluctuations are noticeable in the tables in the hundreds of GeV range, especially for ν_e. At higher energy, where the decay probability of charged pions and kaons is low, the neutrino flux is obtained by allowing all mesons to decay and weighting the contributions by the decay probability. Thus the statistical accuracy of the Monte Carlo calculation is better for $E_{\rm lepton} > 1000$ GeV.

The fluxes of muon neutrinos presented here are somewhat greater at high energy than a preliminary version of this calculation that has been used elsewhere (for example, in Ref. [13]) to calculate the flux of upward, neutrino-induced muons. This is a consequence of changing the treatment of kaon production above 1000 GeV. The difference depends somewhat on angle, but is approximately +10% for $200 < E_\nu < 1000$ GeV and +20% for $1 < E_\nu < 10$ TeV. We estimate that this will lead to a $\approx 3\%$ increase in the predicted flux of neutrino-induced muons with $E_\mu > 3$ GeV.

The quantities presented in Tables IV–VI are intended for comparisons to other calculations of the atmospheric neutrino fluxes. For comparisons to experimental data one should account for the epoch of the solar cycle and the geomagnetic cutoffs at the location of the detector. For this purpose we give in Table VII correction coefficients for upward going neutrinos at four experimental locations and for both minimum and maximum solar activity. These corrections are calculated with a new code for back tracking of cosmic rays in the IGRF magnetic field model [39]. The geomagnetic cutoffs calculated by this code are quite different from the ones used in Ref. [16].

V. CONCLUSION

A. Comparison with other calculations

Figure 6(a) shows our result on the fluxes of vertical muons of energy between 1 and 1000 GeV compared to the fluxes of Refs. [53, 36] and to a collection of experimental data. The slight overestimate of the GeV muon flux in the current calculation is natural, since no geomagnetic or solar cycle corrections are applied to the calculation. The three calculations are in a general agreement, especially when compared to the ~20% or more dispersion of the experimental data. There is a general trend to overestimate slightly the muon flux between 10 and 100 GeV and underestimate it at higher energy. The agreement between the present calculation and Ref. [36] is excellent for muon energy above 100 GeV. This is, however, somewhat coincidental, since the primary cosmic-ray flux of Ref. [36] is significantly different from the one we use (see Fig. 3).

The second panel in Fig. 6 shows a comparison of this calculation (histograms) to measurements of muon fluxes at 0° [66] and 75° [70]. The good agreement over more than 2 orders of magnitude in energy and in flux is a good test of the mechanics of the calculation, such as the treatment of the atmosphere and muon decay and energy loss.

Figure 7 compares our result for the angle averaged fluxes of $\nu_\mu + \bar{\nu}_\mu$ with the results of Refs. [35–37]. Al-

TABLE IV. Fluxes of atmospheric muons as a function of the zenith angle. The values shown are $dN_\mu/d(\ln E_\mu)$ in units of $\rm cm^{-2}\,s^{-1}\,srad^{-1}$.

$\cos\theta$	1.0	0.75	0.50	0.25	0.15	0.05
E_ν (GeV)						
1	4.03×10^{-3}	1.63×10^{-3}	3.78×10^{-4}	3.15×10^{-5}	2.49×10^{-6}	7.16×10^{-7}
2	4.11×10^{-3}	1.98×10^{-3}	6.59×10^{-4}	6.41×10^{-5}	1.27×10^{-5}	1.20×10^{-6}
3	3.59×10^{-3}	2.03×10^{-3}	7.47×10^{-4}	9.46×10^{-5}	2.38×10^{-5}	1.68×10^{-6}
5	2.61×10^{-3}	1.68×10^{-3}	7.87×10^{-4}	1.43×10^{-4}	3.44×10^{-5}	2.92×10^{-6}
10	1.33×10^{-3}	1.02×10^{-3}	6.19×10^{-4}	1.76×10^{-4}	6.27×10^{-5}	5.47×10^{-6}
20	5.29×10^{-4}	4.63×10^{-4}	3.51×10^{-4}	1.55×10^{-4}	7.02×10^{-5}	9.97×10^{-6}
30	2.80×10^{-4}	2.60×10^{-4}	2.18×10^{-4}	1.20×10^{-4}	6.37×10^{-5}	1.24×10^{-5}
50	1.15×10^{-4}	1.15×10^{-4}	1.07×10^{-4}	7.46×10^{-5}	4.97×10^{-5}	1.38×10^{-5}
100	2.94×10^{-5}	3.22×10^{-5}	3.39×10^{-5}	3.09×10^{-5}	2.50×10^{-5}	1.11×10^{-5}
200	6.45×10^{-6}	7.51×10^{-6}	8.90×10^{-6}	9.97×10^{-6}	9.48×10^{-6}	6.27×10^{-6}
300	2.54×10^{-6}	3.04×10^{-6}	3.73×10^{-6}	4.73×10^{-6}	4.75×10^{-6}	3.76×10^{-6}
500	7.33×10^{-7}	9.17×10^{-7}	1.19×10^{-6}	1.70×10^{-6}	1.77×10^{-6}	1.69×10^{-6}
1000	1.30×10^{-7}	1.66×10^{-7}	2.29×10^{-7}	3.69×10^{-7}	3.99×10^{-7}	4.58×10^{-7}
2000	2.24×10^{-8}	2.92×10^{-8}	4.09×10^{-8}	7.02×10^{-8}	7.85×10^{-8}	1.01×10^{-7}
3000	7.66×10^{-9}	9.82×10^{-9}	1.40×10^{-8}	2.63×10^{-8}	2.91×10^{-8}	3.87×10^{-8}
5000	1.96×10^{-9}	2.89×10^{-9}	3.84×10^{-9}	7.32×10^{-9}	7.87×10^{-9}	1.10×10^{-8}

TABLE V. Fluxes of atmospheric ν_μ and $\bar{\nu}_\mu$ as a function of the zenith angle. The values shown are $dN_\nu/d(\ln E_\nu)$ in units of $\mathrm{cm}^{-2}\,\mathrm{s}^{-1}\,\mathrm{srad}^{-1}$.

$\cos\theta$	1.00		0.75		0.50		0.25		0.15		0.05	
E_ν (GeV)	ν_μ	$\bar{\nu}_\mu$	ν_μ	$\bar{\nu}_\mu$	ν_μ	$\bar{\nu}_\mu$	ν_μ	$\bar{\nu}_\mu$	ν_μ	$\bar{\nu}_\mu$	ν_μ	$\bar{\nu}_\mu$
1	1.88×10^{-2}	1.74×10^{-2}	1.99×10^{-2}	1.90×10^{-2}	2.09×10^{-2}	2.08×10^{-2}	2.24×10^{-2}	2.29×10^{-2}	2.35×10^{-2}	2.40×10^{-2}	2.40×10^{-2}	2.38×10^{-2}
2	5.38×10^{-3}	4.97×10^{-3}	5.79×10^{-3}	5.53×10^{-3}	6.31×10^{-3}	6.16×10^{-3}	7.01×10^{-3}	7.08×10^{-3}	7.45×10^{-3}	7.61×10^{-3}	7.78×10^{-3}	7.77×10^{-3}
3	2.47×10^{-3}	2.23×10^{-3}	2.74×10^{-3}	2.55×10^{-3}	3.03×10^{-3}	2.89×10^{-3}	3.47×10^{-3}	3.38×10^{-3}	3.65×10^{-3}	3.68×10^{-3}	3.83×10^{-3}	3.89×10^{-3}
5	9.63×10^{-4}	8.36×10^{-4}	1.07×10^{-3}	9.51×10^{-4}	1.20×10^{-3}	1.07×10^{-3}	1.41×10^{-3}	1.34×10^{-3}	1.50×10^{-3}	1.47×10^{-10}	1.61×10^{-3}	1.63×10^{-3}
10	2.77×10^{-4}	2.21×10^{-4}	2.89×10^{-4}	2.46×10^{-4}	3.31×10^{-4}	2.78×10^{-4}	3.89×10^{-4}	3.55×10^{-4}	4.22×10^{-4}	3.94×10^{-4}	4.74×10^{-4}	$4.59\times^{-4}$
20	7.19×10^{-5}	5.46×10^{-5}	7.65×10^{-5}	6.16×10^{-5}	8.72×10^{-5}	7.18×10^{-5}	1.06×10^{-4}	9.03×10^{-5}	1.15×10^{-4}	1.01×10^{-4}	1.33×10^{-4}	1.23×10^{-4}
30	3.23×10^{-5}	2.34×10^{-5}	3.58×10^{-5}	2.59×10^{-5}	4.01×10^{-5}	3.07×10^{-5}	4.74×10^{-5}	3.95×10^{-5}	5.34×10^{-5}	4.53×10^{-5}	6.10×10^{-5}	5.58×10^{-5}
50	1.16×10^{-5}	7.99×10^{-6}	1.28×10^{-5}	9.07×10^{-6}	1.45×10^{-5}	1.08×10^{-5}	1.77×10^{-5}	1.38×10^{-5}	1.98×10^{-5}	1.60×10^{-5}	2.34×10^{-5}	1.98×10^{-5}
100	2.80×10^{-6}	1.73×10^{-6}	3.11×10^{-6}	1.99×10^{-6}	3.59×10^{-6}	2.39×10^{-6}	4.51×10^{-6}	3.20×10^{-6}	5.00×10^{-6}	3.74×10^{-6}	6.00×10^{-6}	4.80×10^{-6}
200	6.71×10^{-7}	3.67×10^{-7}	7.37×10^{-7}	4.26×10^{-7}	8.62×10^{-7}	5.28×10^{-7}	1.10×10^{-6}	7.04×10^{-7}	1.23×10^{-6}	8.29×10^{-7}	1.49×10^{-6}	1.09×10^{-6}
300	2.69×10^{-7}	1.43×10^{-7}	3.21×10^{-7}	1.75×10^{-7}	3.71×10^{-7}	2.14×10^{-7}	4.82×10^{-7}	3.02×10^{-7}	5.34×10^{-7}	3.40×10^{-7}	6.49×10^{-7}	4.45×10^{-7}
500	8.95×10^{-8}	4.40×10^{-8}	1.02×10^{-7}	5.23×10^{-8}	1.25×10^{-7}	6.64×10^{-8}	1.67×10^{-7}	9.93×10^{-8}	1.82×10^{-7}	1.09×10^{-7}	2.18×10^{-7}	$1.43\times^{-7}$
1000	1.82×10^{-8}	8.37×10^{-9}	2.18×10^{-8}	1.04×10^{-8}	2.72×10^{-8}	1.34×10^{-8}	3.71×10^{-8}	1.91×10^{-8}	4.26×10^{-8}	2.29×10^{-8}	5.07×10^{-8}	3.01×10^{-8}
2000	3.33×10^{-9}	1.50×10^{-9}	4.10×10^{-9}	1.87×10^{-9}	5.53×10^{-9}	2.58×10^{-9}	7.93×10^{-9}	3.88×10^{-9}	9.39×10^{-9}	4.72×10^{-9}	1.14×10^{-8}	6.01×10^{-9}
3000	1.21×10^{-9}	5.33×10^{-10}	1.53×10^{-9}	6.73×10^{-10}	2.08×10^{-9}	9.59×10^{-10}	3.12×10^{-9}	1.44×10^{-9}	3.77×10^{-9}	1.72×10^{-9}	4.75×10^{-9}	2.45×10^{-9}
5000	3.33×10^{-10}	1.41×10^{-10}	4.28×10^{-10}	1.80×10^{-10}	5.98×10^{-10}	2.60×10^{-10}	9.37×10^{-10}	4.20×10^{-10}	$1.14\times^{9}$	5.03×10^{-10}	1.50×10^{-9}	$6.91\times^{-10}$
10000	5.27×10^{-11}	2.21×10^{-11}	6.89×10^{-11}	2.86×10^{-11}	1.01×10^{-10}	4.32×10^{-11}	1.71×10^{-10}	7.07×10^{-11}	2.08×10^{-10}	8.82×10^{-11}	2.91×10^{-10}	1.25×10^{-10}

TABLE VI. Fluxes of atmospheric ν_e and $\bar{\nu}_e$ as a function of the zenith angle. The values shown are $dN_\nu/d(\ln E_\nu)$ in units of $\mathrm{cm}^{-2}\,\mathrm{s}^{-1}\,\mathrm{srad}^{-1}$.

$\cos\theta$	1.00		0.75		0.50		0.25		0.15		0.05	
E_ν (GeV)	ν_e	$\bar{\nu}_e$	ν_e	$\bar{\nu}_e$	ν_e	$\bar{\nu}_e$	ν_e	$\bar{\nu}_e$	ν_e	$\bar{\nu}_e$	ν_e	$\bar{\nu}_e$
1	8.23×10^{-3}	6.51×10^{-3}	9.75×10^{-3}	7.24×10^{-3}	1.15×10^{-2}	8.85×10^{-3}	1.36×10^{-2}	1.02×10^{-2}	1.40×10^{2}	1.15×10^{-2}	1.48×10^{-2}	1.17×10^{-2}
2	2.03×10^{-3}	1.56×10^{-3}	2.54×10^{-3}	2.00×10^{-3}	3.16×10^{-3}	2.46×10^{-3}	4.09×10^{-3}	3.26×10^{-3}	$4.58i\times10^{-3}$	3.55×10^{-3}	4.89×10^{-3}	3.83×10^{-3}
3	7.87×10^{-4}	6.66×10^{-4}	1.04×10^{-3}	8.17×10^{-4}	1.36×10^{-3}	1.11×10^{-3}	1.90×10^{-3}	1.48×10^{-3}	2.16×10^{-3}	1.68×10^{-3}	2.38×10^{-3}	1.90×10^{-3}
5	2.50×10^{-4}	2.02×10^{-4}	3.09×10^{-4}	2.58×10^{-4}	4.35×10^{-4}	3.52×10^{-4}	6.72×10^{-4}	5.42×10^{-4}	7.93×10^{-4}	6.50×10^{-4}	9.47×10^{-4}	7.54×10^{-4}
10	4.15×10^{-5}	3.68×10^{-5}	5.99×10^{-5}	4.83×10^{-5}	8.60×10^{-5}	7.18×10^{-5}	1.46×10^{-4}	1.21×10^{-4}	1.88×10^{-4}	1.56×10^{-4}	2.47×10^{-4}	2.02×10^{-4}
20	7.77×10^{-6}	6.47×10^{-6}	1.01×10^{-5}	8.39×10^{-6}	1.57×10^{-5}	1.30×10^{-5}	2.89×10^{-5}	2.35×10^{-5}	3.98×10^{-5}	3.22×10^{-5}	5.84×10^{-5}	4.70×10^{-5}
30	2.82×10^{-6}	2.35×10^{-6}	3.66×10^{-6}	3.03×10^{-6}	5.76×10^{-6}	4.61×10^{-6}	1.10×10^{-5}	9.05×10^{-6}	1.52×10^{-5}	1.27×10^{-5}	2.53×10^{-5}	1.99×10^{-5}
50	7.44×10^{-7}	6.25×10^{-7}	1.05×10^{-6}	7.80×10^{-7}	1.51×10^{-6}	1.22×10^{-6}	2.97×10^{-6}	2.43×10^{-6}	4.26×10^{-6}	3.65×10^{-6}	7.28×10^{-6}	6.25×10^{-6}
100	1.48×10^{-7}	1.16×10^{-7}	1.77×10^{-7}	1.52×10^{-7}	2.67×10^{-7}	1.96×10^{-7}	4.89×10^{-7}	4.18×10^{-7}	7.43×10^{-7}	6.30×10^{-7}	1.40×10^{-6}	1.12×10^{-6}
200	2.46×10^{-8}	2.37×10^{-8}	3.59×10^{-8}	2.55×10^{-8}	5.01×10^{-8}	3.87×10^{-8}	8.48×10^{-8}	6.79×10^{-8}	1.16×10^{-7}	9.16×10^{-8}	2.43×10^{-7}	1.87×10^{-7}
300	1.14×10^{-8}	7.41×10^{-9}	1.25×10^{-8}	1.03×10^{-8}	2.01×10^{-8}	1.22×10^{-8}	3.05×10^{-8}	2.49×10^{-8}	4.19×10^{-8}	3.34×10^{-8}	7.62×10^{-8}	6.28×10^{-8}
500	3.29×10^{-9}	2.15×10^{-9}	3.83×10^{-9}	2.63×10^{-9}	5.26×10^{-9}	3.90×10^{-9}	8.42×10^{-9}	6.94×10^{-9}	1.11×10^{-8}	8.57×10^{-9}	2.00×10^{-8}	1.62×10^{-8}
1000	5.86×10^{-10}	3.67×10^{-10}	7.46×10^{-10}	4.58×10^{-10}	9.70×10^{-10}	6.29×10^{-10}	1.52×10^{-9}	9.78×10^{-10}	1.98×10^{-9}	1.47×10^{-9}	3.30×10^{-9}	2.61×10^{-9}
2000	1.00×10^{-10}	6.23×10^{-11}	1.26×10^{-10}	7.80×10^{-11}	1.75×10^{-10}	1.14×10^{-10}	2.68×10^{-10}	1.78×10^{-10}	3.86×10^{-10}	2.42×10^{-10}	5.20×10^{-10}	4.02×10^{-10}
3000	3.51×10^{-11}	2.15×10^{-11}	4.50×10^{-11}	2.71×10^{-11}	6.42×10^{-11}	4.06×10^{-11}	1.01×10^{-10}	6.45×10^{-11}	1.28×10^{-10}	8.35×10^{-11}	2.01×10^{-10}	1.40×10^{-10}
5000	9.24×10^{-12}	5.45×10^{-12}	1.18×10^{-11}	7.01×10^{-12}	1.73×10^{-11}	1.07×10^{-11}	2.86×10^{-11}	1.79×10^{-11}	3.55×10^{11}	2.25×10^{-11}	5.41×10^{11}	3.40×10^{-11}
10000	1.47×10^{-12}	8.46×10^{-13}	1.90×10^{-12}	1.13×10^{-12}	2.79×10^{-12}	1.67×10^{-12}	4.84×10^{-12}	2.93×10^{-12}	6.05×10^{-12}	3.63×10^{-12}	8.76×10^{-12}	5.38×10^{-12}

TABLE VII. Geomagnetic corrections for upward going muon neutrinos plus antineutrinos for several experimental locations.

Location		$\odot_{max}$						$\odot_{min}$					
	$\cos\theta$	-1.00	-0.75	-0.50	-0.25	-0.15	-0.05	-1.00	-0.75	-0.50	-0.25	-0.15	-0.05
	E_ν (GeV)												
Kamioka	1.0	0.75	0.70	0.69	0.64	0.60	0.56	0.75	0.70	0.69	0.64	0.61	0.57
	2.0	0.92	0.88	0.87	0.83	0.78	0.75	0.92	0.88	0.88	0.84	0.79	0.75
	3.0	0.99	0.96	0.95	0.90	0.88	0.85	1.00	0.96	0.96	0.90	0.88	0.85
	5.0	1.00	0.98	1.00	0.94	0.94	0.93	1.00	0.98	1.00	0.94	0.94	0.93
IMB	1.0	0.89	0.90	0.91	0.91	0.87	0.78	0.98	0.99	1.00	1.00	0.94	0.84
	2.0	0.96	0.96	0.97	0.97	0.95	0.90	0.98	0.99	1.00	1.00	0.97	0.91
	3.0	1.00	0.98	1.00	0.98	0.99	0.96	1.00	0.99	1.00	1.00	0.99	0.96
	5.0	1.00	0.99	1.00	0.99	0.99	0.99	1.00	1.00	1.00	1.00	0.99	0.99
GS/Frejus	1.0	0.86	0.87	0.87	0.82	0.75	0.68	0.92	0.93	0.92	0.86	0.79	0.72
	2.0	0.96	0.95	0.96	0.95	0.88	0.83	0.98	0.97	0.98	0.96	0.90	0.84
	3.0	1.00	0.98	1.00	0.97	0.95	0.91	1.00	1.00	1.00	0.97	0.96	0.91
	5.0	1.00	0.99	1.00	0.98	0.97	0.96	1.00	1.00	1.00	0.99	0.98	0.97
SNO/Soudan	1.0	0.89	0.90	0.90	0.92	0.89	0.83	0.98	0.99	1.00	1.00	0.97	0.89
	2.0	0.96	0.96	0.97	0.98	0.96	0.93	0.98	0.99	1.00	1.00	0.98	0.94
	3.0	1.00	0.99	1.00	0.99	0.99	0.98	1.00	1.00	1.00	1.00	1.00	0.98
	5.0	1.00	1.00	1.00	1.00	0.99	0.99	1.00	1.00	1.00	1.00	1.00	0.99

though the general agreement between the four calculations is not bad, there are significant differences in the important energy range between 10 and 1000 GeV that cause differences of order 10 – 15 % in the calculated flux of upward going neutrino induced GeV muons.

B. Uncertainty in the neutrino flux

Uncertainties in the calculated neutrino intensity arise from lack of precise knowledge of the input quantities, which are the primary spectrum and the inclusive cross section for production of pions and kaons by hadronic interactions in the atmosphere. Because the relative contributions of kaons and pions to the neutrino flux depends both on energy and on angle, it is not possible to assign a single estimate of the uncertainty to the calculation. We have estimated the primary spectrum uncertainty by a single overall ±15%.[1] If we also were to assign a similar single uncertainty to the production cross sections, then we would estimate a overall uncertainty of ±21% as in Ref. [13].

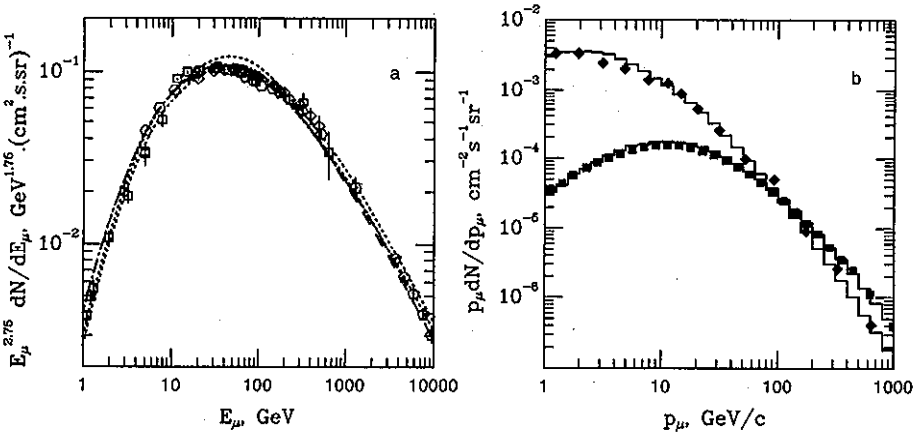

FIG. 6. (a) Vertical muon fluxes calculated in Refs. [53] (dotted lines with high and low normalization) and [36] are compared with the current calculation (solid line) and experimental data. The data points are from Refs. [66] (squares), [67] (hexagons), [68] (diamonds), and [69] (pentagons). (b) Muon flux at $\theta = 0°$ (diamonds) [66] and $\theta = 75°$ (squares) [70] compared to the current calculation.

[1]The uncertainties in the primary spectrum may also change with energy if it is possible to choose one of the two [19, 20] 10 – 100 GeV measurements over the other.

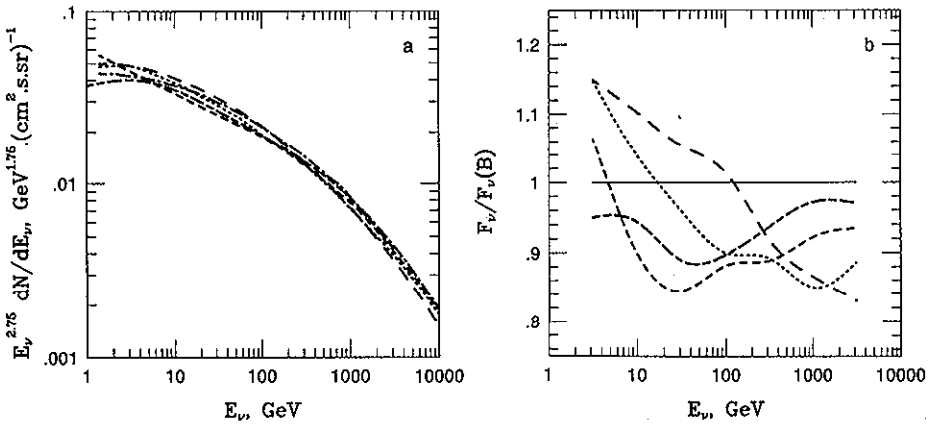

FIG. 7. (a) Angle average fluxes of $\nu_\mu + \bar{\nu}_\mu$ calculated by Volkova [35] (short dashed), Butkevich *et al.* [36] (long dashed), Mitsui *et al.* [37] (dotted), and Honda *et al.* [38] (short-long dashed) compared to the calculation (dash-dotted). (b) To expand the comparison, we show the same information on a linear scale by plotting the ratio of each calculated flux F_ν from (a) to our calculation, $F_\nu(B)$. The line coding is the same except for the reference calculation.

Approximately 70% of neutrino-induced muons are produced by neutrinos with $10 \leq E(\nu_\mu) \leq 1000$ GeV. If we focus on this energy region, about half the (vertical) neutrinos come from pions and half from kaons (a larger proportion of kaons above 100 GeV and a smaller proportion below 100 GeV). Thus if there is a $\pm 12\%$ uncertainty in $Z_{p\pi^\pm}$ and an independent $\pm 17\%$ uncertainty in $Z_{pK^\pm}$, then these contribute, respectively, $\pm 6\%$ and $\pm 8.5\%$. Combining these uncertainties with the $\pm 15\%$ uncertainty in the primary spectrum as if they were all statistical errors, we would estimate a $\pm 18\%$ uncertainty. For illustration, let us call this nominal result 1 ± 0.18.

Another possibility is to use the measured muon spectrum as a constraint. As discussed before, this flux depends only weakly on the properties of kaon production and essentially measures the product of the primary flux with $Z_{p\pi^\pm}$. Since the muon on average takes more energy than the neutrino in $\pi \to \mu\nu_\mu$, the relevant range of muon energies is $30 < E_\mu < 3000$ GeV. From Fig. 6, we estimate this uncertainty as $\pm 10\%$. Combining this uncertainty with the uncertainty in $Z_{pK^\pm}$ as if they were uncorrelated statistical errors, we find an overall systematic error of $\pm 14\%$.

The errors are not statistical, however. For example, if it were determined that the higher set [19] of primary spectrum measurements below 100 GeV were correct and the spectral index could be determined with sufficient precision to extrapolate to higher energy, we would shift the central value upward by 12% and assign a smaller error $\sim \pm 10\%$ to the spectrum. Relative to the nominal estimate above, our new estimate would be 1.12 ± 0.16, assuming the other uncertainties remain unchanged.

Finally, by a similar argument, if we shift the estimate of $Z_{pK^\pm}$ downward by 20%, for example, then (always averaging over the energy range relevant for vertical upward neutrino-induced muons) the central value would drop from unity to 0.9. If the uncertainties remain as initially assumed, the new estimate would be 0.9 ± 0.16.

ACKNOWLEDGMENTS

We are grateful for helpful discussions with D. Michael and S. Mikheyev. This work was supported in part by the U.S. Department of Energy (T.K.G. and T.S.) and by the INFN (P.L.).

[1] IBM Collaboration, R. Becker-Szendy *et al.*, Phys. Rev. Lett. **69**, 1010 (1992).
[2] M. Mori *et al.*, Phys. Lett. B **210**, 89 (1991).
[3] M.M. Boliev *et al.*, in *Proceedings of the 3rd International Workshop on Neutrino Telescopes*, Venice, Italy, 1991, edited by M. Baldo-Ceolin (Istituto Nazionale di Fisica Nucleare, Padova, 1991), p. 235.
[4] Frejus Collaboration, K. Daum *et al.*, Z. Phys. C **66**, 417 (1995).
[5] MACRO Collaboration, D. Michael *et al.*, in *TAUP 93*, Proceedings of the Third International Workshop on Theoretical and Phenomenological Aspects of Underground Physics, Asswergi, Italy, edited by C. Arpesella *et al.* [Nucl. Phys. B (Proc. Suppl.) **35** (1994)].
[6] LVD Collaboration M. Aglietta *et al.*, Astropart. Phys. **3**, 311 (1995).
[7] C.V. Achar *et al.*, Phys. Lett. **18**, 196 (1965); **19**, 78 (1965).
[8] F. Reines *et al.*, Phys. Rev. Lett. **15**, 429 (1965).
[9] Kam-II Collaboration, K.S. Hirata *et al.*, Phys. Lett. B **280**, 146 (1992); Y. Fukuda *et al.*, *ibid.* **335**, 237 (1994).
[10] IMB Collaboration, R. Becker-Szendy *et al.*, Phys. Rev. D **46**, 3720 (1992). See also D. Casper *et al.*, Phys. Rev. Lett. **66**, 2561 (1991).
[11] W. Lohmann, R. Kopp, and R. Voss, CERN Yellow Report No. EP/85-03 (unpublished).

[12] Paolo Lipari and Todor Stanev, Phys. Rev. D **44**, 3543 (1991).
[13] W. Frati, T.K. Gaisser, A.K. Mann, and Todor Stanev, Phys. Rev. D **48**, 1140 (1993).
[14] IMB Collaboration, R. Becker-Szendy *et al.*, in *Neutrino 94* [4], p. 331.
[15] Paolo Lipari, Maurizio Lusignoli, and Francesca Sartogo, Phys. Rev. Lett. **22**, 4384 (1995).
[16] Giles Barr, T.K. Gaisser, and Todor Stanev, Phys. Rev. D **39**, 3532 (1989).
[17] J. Engel *et al.*, Phys. Rev. D **46**, 5013 (1992).
[18] T.K. Gaisser and Todor Stanev (unpublished).
[19] W.R. Webber, R.L. Golden, and S.A. Stephens, in *Proceedings of the 20th International Cosmic Ray Conference*, Moscow, USSR, 1987, edited by V. Kozyarivsky *et al.* (Nauka, Moscow, 1987), Vol. 1, p. 325.
[20] E.-S. Seo *et al.*, Astrophys. J. **378**, 763 (1991).
[21] M.J. Ryan, J.F. Ormes, and V.K. Balasubramanyan, Phys. Rev. Lett. **28**, 985 (1972); **28**, 1497E (1972).
[22] I.P. Ivanenko *et al.*, in *Cosmic Ray Conference*, Proceedings of the 23rd International Conference, edited by D.A. Leahy *et al.* (University of Calgary, Calgary, Canada, 1993), Vol. 2, p. 25.
[23] K. Asakimori *et al.*, in *Cosmic Ray Conference* [22], p. 21.
[24] K. Asakimori *et al.*, in *Cosmic Ray Conference* [22], p. 25.
[25] Y. Kawamura *et al.*, Phys. Rev. D **40**, 729 (1989).
[26] V.I. Zatsepin *et al.*, in *Cosmic Ray Conference* [22], p. 130.
[27] J. Dwyer *et al.*, in *Cosmic Ray Conference* [22], Vol. 1, p. 587.
[28] J.J. Engelmann *et al.*, Astron. Astrophys. **233**, 96 (1990).
[29] M. Simon *et al.*, Astrophys. J. **239**, 712 (1980).
[30] J. Buckley *et al.*, in *Cosmic Ray Conference* [22], Vol. 1, p. 599.
[31] D. Müller *et al.*, Astrophys. J. **374**, 356 (1991); S.P. Swordy, J. L'Heureux, P. Meyer, and D. Müller, *ibid.* **403**, 658 (1993).
[32] M. Ichimura *et al.*, Phys. Rev. D **48**, 1949 (1993).
[33] J.A. Simpson, Annu. Rev. Nucl. Part. Sci. **33**, 323 (1983).
[34] S. Swordy, in *Cosmic Ray Conference* [22], p. 243.
[35] L.V. Volkova, Yad. Fiz. **31**, 1510 (1980) [Sov. J. Nucl. Phys. **31**, 784 (1980)].
[36] A.V. Butkevich, L.G. Dedenko, and I.M. Zheleznykh, Yad. Fiz. **50**, 142 (1989) [Sov. J. Nucl. Phys. **50**, 90 (1989)].
[37] K. Mitsui, Y. Minorikawa, and H. Komori, Nuovo Cimento **C9**, 995 (1986).
[38] M. Honda, T. Kajita, K. Kasahara, and S. Midorikawa, Phys. Rev. D **52**, 4985 (1995).
[39] P. Lipari and T. Stanev (unpublished).
[40] E. Stenlund and I. Otterlund, CERN Report No. CERN/EP/82-42 (unpublished).
[41] T. Eichten *et al.*, Nucl. Phys. **B44**, 333 (1972).
[42] J.V. Allaby *et al.*, CERN Yellow Report No. 70-12 (unpublished).
[43] W.D. Walker, in *High Energy Physics - 1980*, Proceedings of the 20th International Conference, Madison, Wisconsin, edited by L. Durand and L.G. Pondrom, AIP Conf. Proc. No. 68 (AIP, New York, 1980), p. 77.
[44] D.S. Barton *et al.*, Phys. Rev. D **27**, 2580 (1983).
[45] T.K. Gaisser, R.J. Protheroe, and Todor Stanev, in *Proceedings of the 18th International Cosmic Ray Conference*, Bangalore, India, 1983, edited by N. Durgaprasad *et al.* (TIFR, Bombay, 1983), Vol. 5, p. 174 (Fig. 1 of this paper is incorrectly plotted).
[46] Thomas K. Gaisser, *Cosmic Rays and Particle Physics* (Cambridge University Press, Cambridge, England 1990).
[47] Paolo Lipari, Astropart. Phys. **1**, 195 (1993).
[48] T.K. Gaisser, P. Lipari, and T. Stanev, in *Cosmic Ray Conference* [22], Vol. 4, p. 495.
[49] A.E. Brenner *et al.*, Phys. Rev. D **26**, 1497 (1982).
[50] M. Aguilar-Benitez *et al.*, Z. Phys. C **50**, 405 (1991).
[51] E. Yen, Phys. Rev. D **10**, 836 (1974).
[52] Y. Minorikawa and K. Mitsui, Lett. Nuovo Cimento **41**, 333 (1984).
[53] L.V. Volkova, G.T. Zatsepin, and L.A. Kuz'michev, Yad. Fiz. **29**, 1252 (1979).
[54] R.S. Fletcher *et al.*, in *Cosmic Ray Conference* [22], Vol. 4, p. 40.
[55] D.H. Perkins, Astropart. Phys. **2**, 249 (1994).
[56] A.M. Hillas, *Proceedings of the 16th International Cosmic Ray Conference* (Institute Cosmic Ray Research, Tokyo, 1979), Vol. 8, p. 7.
[57] R.S. Fletcher *et al.*, Phys. Rev. D **50**, 5710 (1994).
[58] G.J. Marmer *et al.*, Phys. Rev. **179**, 1294 (1969).
[59] D. Antreasyan *et al.*, Phys. Rev. D **19**, 764 (1979).
[60] P. Skubic *et al.*, Phys. Rev. D **18**, 3115 (1978).
[61] K. Jaeger, D. Colley, L. Hyman, and J. Rest, Phys. Rev. D **11**, 2405 (1975).
[62] M. Bourquin *et al.*, Nucl. Phys. **B153**, 13 (1979).
[63] M. Antinucci *et al.*, Lett. Nuovo Cimento **6**, 121 (1973).
[64] F. Tagaki, Prog. Theor. Phys. **65**, 1350 (1981).
[65] S. Tasaka *et al.*, Phys. Rev. D **25**, 1765 (1982).
[66] O.C. Allkofer, K. Carstensen, and W.D. Dau, Phys. Lett. **36B**, 425 (1971).
[67] B.C. Rastin, J. Phys. G **10**, 1609 (1984).
[68] C.A. Ayre *et al.*, J. Phys. G **1**, 584 (1975).
[69] I.P. Ivanenko *et al.*, in *Proceedings of the 19th International Cosmic Ray Conference*, La Jolla, California, 1985, edited by F.C. Jones, J. Adams, and G.M. Mason, NASA Conf. Publ. No. 2376 (Goddard Space Flight Center, Greenbelt, MD, 1985), Vol. 8, p. 210.
[70] H. Jokisch *et al.*, Phys. Rev. D **19**, 1368 (1979).